
Computational Geosciences **8:** 21–47, 2004.
© 2004 *Kluwer Academic Publishers. Printed in the Netherlands.*

Forward and inverse problems in modeling of multiphase flow and transport through porous media

S.B. Hazra [a], H. Class [b], R. Helmig [b] and V. Schulz [a]

[a] *Department of Mathematics, University of Trier, D-54286 Trier, Germany*
E-mail: hazra@uni-trier.de
[b] *Institute of Hydraulic Engineering, University of Stuttgart, Pfaffenwaldring 61, D-70569 Stuttgart, Germany*

Received November 2002; accepted 26 January 2004

The paper deals with numerical simulation techniques for forward and inverse modelling in multiphase (multicomponent) flow through porous media. The forward simulation software system MUFTE-UG uses recent discretization techniques and fast solvers. The efficient integration of optimization strategies for the solution of the inverse problems is demonstrated in detail and also applied to practical numerical examples.

Keywords: multiphase flow, multiple shooting, numerical parameter identification, porous media, reduced Gauss–Newton technique

1. Introduction

On the way from field measurements to the realistic model for heterogeneous porous media, which helps in development and optimization of ground water management and remediation techniques, inverse modeling plays an important role. The questions arising therein are of interdisciplinary nature, stemming from hydrodynamic modeling and numerical mathematics. The modeling of flow and transport processes in porous media is described by a system of partial differential equations which can be discretized and solved efficiently by the use of multigrid methods. In case of inverse modeling, the parameters (e.g., permeability, porosity or diffusion coefficient), which in many cases depend on space coordinates, are to be determined on the basis of field measurements.

In this paper, we explain the numerical methods for inverse modeling which have recently been developed for non-stationary multiphase systems. It has been possible to integrate the optimization software into the simulation tool MUFTE-UG [20]. The applicability of the method is tested and validated by using practical experimental data from VEGAS, University of Stuttgart. It is shown that hysteresis effects play an important role in multiphase flow and transport processes, which so far have not been taken into account in our numerical model. This will be our future direction of research.

The paper is organized as follows: We discuss the software tool MUFTE-UG in the next section. In section 3, we discuss the general physical and mathematical model for multiphase flow through porous media and the discretization method of the model equations in the subsequent section. In section 5, we describe in detail the parameter identification technique. In section 6, we discuss the results obtained by using this technique for both isothermal as well as non-isothermal multiphase flow. Our conclusions are drawn in section 7.

2. The software system MUFTE_UG

New discretization techniques and fast solvers for the simulation of multiphase–multicomponent flow in porous and highly heterogeneous media are being developed by interdisciplinary teams at the Institute of Hydraulic Research (IWS), University of Stuttgart, and at the Technical Simulation Group of the Interdisciplinary Center for Scientific Computing, University of Heidelberg (IWR). The platform for this work is the numerical simulation program MUFTE_UG, which combines the physical procedure and the discretization techniques of the program system MUFTE (Multiphase Flow, Transport and Energy Model, IWS) with the solvers and multigrid techniques of the program system UG (Unstructured Grids, IWR) (see figure 1). In MUFTE_UG [20], all modules are made available in such a way that they can be combined easily. A good overview of the available isothermal and nonisothermal MUFTE modules in combination with the solution and discretization techniques offered in UG can be found, for example, in [3,10].

3. Physical–mathematical model

The mathematical formulation of a multiphase flow and transport system in a porous medium requires a system of equations that is capable to describe the relevant

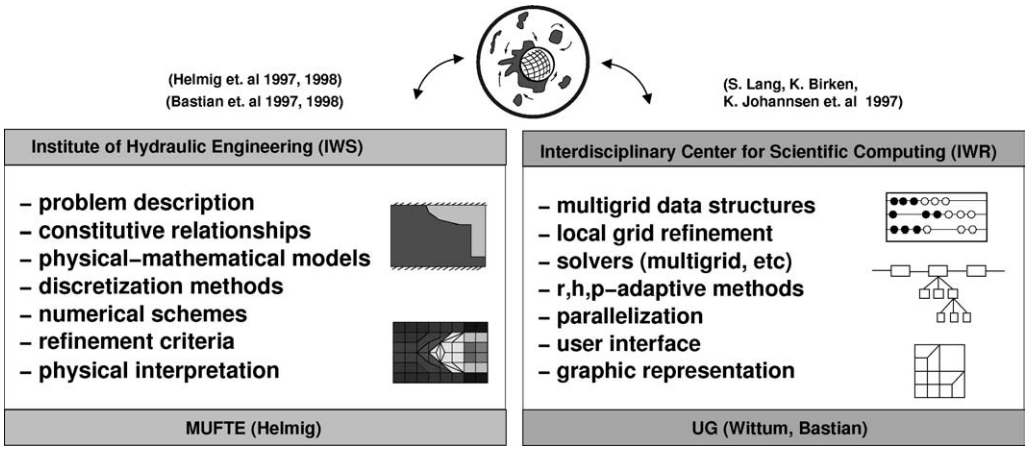

Figure 1. MUFTE_UG as a joint venture between IWS and IWR [20].

physical processes appropriately. Depending on a given problem, as a preliminary step one has to build up a conceptual model which must reproduce the essential characteristic properties of the system behavior. A major distinction is made between multiphase systems and multiphase multicomponent systems. A multiphase system consists of two or more fluid phases. In the case of a multiphase multicomponent system, the phases may be composed of several components and the components may exchange from one phase into another. Such mass transfer processes are, for example, evaporation, condensation, dissolution, and degassing. These are coupled with an exchange of thermal energy between the phases. Thus, an energy balance is necessary in order to take that into account. In the following, we will first present the general form of the multiphase flow differential equation. On the basis of that, we describe the equations and properties of an isothermal two-phase system and afterwards extend this to a nonisothermal two-phase two-component water–gas model concept. Then, we introduce the constitutive relationships and closure relations.

3.1. General form of the multiphase flow equations

In the Eulerian approach, the continuity equation for multiphase flow in porous media for a phase α is given by

$$\int_G \left[\frac{\partial(\phi S_\alpha \varrho_\alpha)}{\partial t} + \nabla \cdot (\varrho_\alpha \mathbf{v}_\alpha) \right] \mathrm{d}G = 0. \tag{3.1}$$

Here, ϕ stands for the porosity, S_α for the saturation, and ϱ_α for the mass density, where the index α identifies the respective fluid phase. $\mathbf{v}_\alpha$ is the flow velocity of phase α averaged over the cross section of the porous medium. Note that this is not the mean velocity $\mathbf{v}_{a,\alpha}$ of the water molecules, since the latter is related to the Darcy velocity by

$$\mathbf{v}_\alpha = \mathbf{v}_{a,\alpha}\phi. \tag{3.2}$$

Darcy's law for single phase flow is

$$\mathbf{v} = -\frac{\mathbf{K}}{\mu} \cdot (\nabla p - \varrho \mathbf{g}), \tag{3.3}$$

where p is the phase pressure, $\mathbf{K}$ the intrinsic permeability tensor of the porous medium, μ the dynamic viscosity of the fluid, and $\mathbf{g}$ the vector of gravitational acceleration. For a multiphase system, the Darcy law (equation (3.3)) can be extended by considering the relative permeability $k_{r\alpha}$ of the phases, e.g., [19], such that the Darcy velocity for a phase α is obtained by

$$\mathbf{v}_\alpha = -\frac{k_{r\alpha}}{\mu_\alpha}\mathbf{K} \cdot (\nabla p_\alpha - \varrho_\alpha \mathbf{g}). \tag{3.4}$$

The term $k_{r\alpha}/\mu_\alpha$ is commonly called the mobility λ_α of phase α.

By using Darcy's law as a reduced form of the momentum equation in porous media, it is possible to decouple the calculation of the phase velocities from the continuity

equation. Inserting equation (3.4) into equation (3.1), adding a source/sink term q_α for phase α, and writing in differential form yields the general form of the multiphase flow equation:

$$\frac{\partial(\phi S_\alpha \varrho_\alpha)}{\partial t} - \nabla \cdot \left(\varrho_\alpha \lambda_\alpha \mathbf{K} \cdot (\nabla p_\alpha - \varrho_\alpha \mathbf{g})\right) - \varrho_\alpha q_\alpha = 0. \tag{3.5}$$

3.1.1. Two-phase flow

Now, we consider a two-phase system. The fluid phase, which has the higher affinity to the porous medium, is the wetting phase w, the second phase is the non-wetting phase n. We always have water as the wetting and gas as the non-wetting phase. Then, equation (3.5) represents a system of two coupled differential equations, which is completed by

$$\sum_\alpha S_\alpha = 1, \tag{3.6}$$

the linkage of the phase pressures via the capillary pressure p_c

$$p_c = p_n - p_w = f(S), \tag{3.7}$$

and additional state relations for the density $\varrho(p)$, for example, Ideal Gas law, viscosity $\mu(p)$ and relative permeability $k_r(S)$. The system exhibits a high degree of nonlinearity, mainly caused by the nonlinear dependence of the capillary pressure and the relative permeability on the saturation. This is reinforced by a strong variation of these constitutive relationships due to heterogeneities.

Pressure-saturation formulation. The choice of the primary variables can be made in different ways. The method we use here is the pressure-saturation formulation. The two unknowns are the pressure of the wetting phase p_w and the saturation of the non-wetting phase S_n, respectively vice versa p_n and S_w. The following reformulations should be made for terms from equation (3.5):

$$\nabla p_n = \nabla(p_w + p_c), \tag{3.8}$$

$$\frac{\partial S_w}{\partial t} = \frac{\partial}{\partial t}(1 - S_n) = -\frac{\partial S_n}{\partial t}. \tag{3.9}$$

Then, we get for the wetting phase (water)

$$-\phi \varrho_w \frac{\partial S_n}{\partial t} - \nabla \cdot \left(\varrho_w \lambda_w \mathbf{K} \cdot (\nabla p_w - \varrho_w \mathbf{g})\right) - \varrho_w q_w = 0, \tag{3.10}$$

and for the non-wetting phase (gas or NAPL)

$$\phi \frac{\partial(\varrho_n S_n)}{\partial t} - \nabla \cdot \left(\varrho_n \lambda_n \mathbf{K} \cdot (\nabla p_w + \nabla p_c - \varrho_n \mathbf{g})\right) - \varrho_n q_n = 0. \tag{3.11}$$

Note that we take the porosity ϕ out of the time derivative term since we assume it to be constant. We do the same with the wetting phase density ϱ_w due to the assumption

of water being incompressible. If the non-wetting phase is a gaseous phase, we have to consider a density varying with pressure.

Some alternatives exist to the pressure-saturation formulation, for an overview see, e.g., [19]. One of them is the pressure formulation with both phase pressures as unknowns. This formulation takes advantage of the monotonic behavior of the capillary pressure as a function of saturation, which is the precondition for the existence of an inverse function $S = g(p_c)$. However, the disadvantage of the pressure formulation appears when the gradient of the capillary pressure becomes small $\mathrm{d}p_c/\mathrm{d}S \approx 0$. As will be shown later, this case normally occurs for high water saturations. For two incompressible fluids, it is also possible to use the fractional flow formulation [19].

3.1.2. Nonisothermal water–gas systems

In the following we extend the isothermal two-phase flow model to a nonisothermal water–gas system containing the phases water and gas (phase $\alpha \in \{w, g\}$)[1] as well as the components water and air[2] (denoted by the superscripts wa respectively ai, component $K \in \{wa, ai\}$). A more detailed presentation of the nonisothermal model concept implemented in the program system MUFTE_UG [20] is given by Class et al. (2002) [10] and Class (2001) [9].

The system of equations includes two mass balances, one for each component, and a single energy balance. Note that we assume local thermal equilibrium. Chemical or biological effects are not considered. The pressure and temperature ranges for which the model concept is designed are $\approx$ 1–5 bar and $\approx$ 0–200°C.

We formulate the balance equations for each mass component by multiplying the terms in equation (3.5) with the corresponding mole fractions of the components in the phases and by summing up over the phases. Note that we additionally consider a diffusive flux term in the gas phase. Furthermore, the balance equations are molar, which is why we distinguish between the molar density $\varrho_{\mathrm{mol},\alpha}$ and the mass density $\varrho_{\mathrm{mass},\alpha}$.

Mass balances:

$$\phi \frac{\partial(\sum_\alpha \varrho_{\mathrm{mol},\alpha} x_\alpha^K S_\alpha)}{\partial t} - \sum_\alpha \nabla \cdot \left\{ \frac{k_{r\alpha}}{\mu_\alpha} \varrho_{\mathrm{mol},\alpha} x_\alpha^K \mathbf{K}(\nabla p_\alpha - \varrho_{\mathrm{mass},\alpha}\mathbf{g}) \right\}$$
$$-\nabla \cdot \left\{ D_{pm} \varrho_{\mathrm{mol},g} \nabla x_g^K \right\} - q^K = 0, \quad K \in \{w, a\},\ \alpha \in \{w, g\}. \tag{3.12}$$

The diffusion coefficient D_{pm}^K is obtained by

$$D_{pm} = \tau \phi S_g D_g^{aw}, \tag{3.13}$$

where τ is the tortuosity of the porous medium and D_g^{aw} the binary diffusion coefficient of air/steam.

[1] We overload subscript w with both meanings *water* and *wetting phase*, as in our context the wetting phase is always water.

[2] We are well aware that air consists of several components. However, we neglect this for the sake of simplicity.

Thermal energy:

$$\phi \frac{\partial(\sum_\alpha \varrho_{\text{mass},\alpha} u_\alpha S_\alpha)}{\partial t} + (1-\phi)\frac{\partial \varrho_s c_s T}{\partial t} - \nabla \cdot (\lambda_{pm} \nabla T)$$
$$- \sum_\alpha \nabla \cdot \left\{ \frac{k_{r\alpha}}{\mu_\alpha} \varrho_{\text{mass},\alpha} h_\alpha \mathbf{K}(\nabla p_\alpha - \varrho_{\text{mass},\alpha}\mathbf{g}) \right\}$$
$$- \sum_K \nabla \cdot \left\{ D_{pm} \varrho_{\text{mol},g} h_g^K M^K \nabla x_g^K \right\} - q^h = 0, \quad K \in \{w, a\},\ \alpha \in \{w, g\}. \quad (3.14)$$

c_s is the specific heat capacity of the soil grains. u_α and h_α denote the specific internal energy, respectively enthalpy of the phases. λ_{pm} represents the heat conductivity averaged over the whole fluid-filled porous medium.

Mass/energy transfer and local phase state. The nonisothermal systems that we typically investigate are characterized by the possibility of mass transfer and phase appearance/disappearance due to mass transfer processes like evaporation, condensation, dissolution, and degassing.

This is sketched in figure 2. In particular, condensation and evaporation are coupled with a strong exchange of thermal energy. When a phase appears or disappears locally, the number and the combination of the fluid phases being present at that point change. Therefore, we introduce the term phase state. In a water–gas system, there are three possible phase states (see table 1). The ratios of the components K in the fluid phases α are expressed by mole fractions x_α^K. The mole fraction of dissolved air in the water phase is very small and can be described by Henry's law. The mole fraction of steam in the gas phase is determined by the saturation vapor pressure, which is a function of temperature. Note that this works only as long as water is also present as a liquid phase. If the water phase is not there or has disappeared, for example, due to evaporation, the mole fraction of steam in the gas phase x_g^{wa} is an independent variable. In such a case, we choose x_g^{wa} to be one of the primary variables.

We can see that the set of three primary variables for the three equations is not constant and depends on the local phase state. Table 1 lists the possible phase states

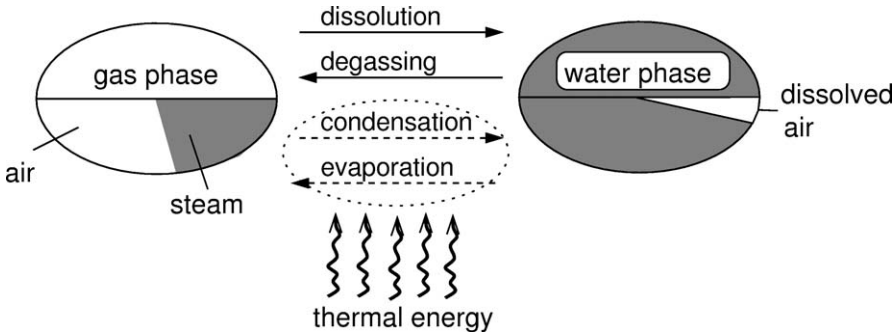

Figure 2. Phases, components, and transfer processes of mass and energy between the fluid phases (modified according to [9]).

Table 1
Phase states and corresponding set of primary variables.

Phase state	Primary variables
both phases	S_w, p_g, T
gas phase	x_g^{wa}, p_g, T
water phase	x_w^{ai}, p_g, T

and the corresponding primary variables. Note, that we use p_g as a primary variable for all phase states, also for the state "water phase", although p_g is not a physically defined parameter here. We can do so by interpreting p_g as the total pressure of the system which is coupled to p_w via the capillary pressure-saturation function. Changes of the local phase states, i.e., the appearance or disappearance of fluid phases, must be recognized by the model. This requires the formulation of an algorithm providing criteria for the indication of a phase state change. Phase disappearance is simply indicated by negative values of the corresponding saturations. An appearance of the phases requires a distinction in the algorithm between the case when liquid water appears and the case when the gas phase appears. Water appears when the partial pressure of steam in the gas phase exceeds the saturation vapor pressure

$$p_g^{wa} = x_g^{wa} p_g > p_{\text{sat}}^{wa}(T). \tag{3.15}$$

Gas appears as a phase when the sum of the (hypothetical) vapor pressures exceeds the total pressure given by p_g, which in this case is also a hypothetical gas phase pressure

$$H_w^{ai} x_w^{ai} + p_{\text{sat}}^{wa} > p_g, \tag{3.16}$$

where H_w^{ai} is Henry's constant for the dissolution of air in water.

3.2. Constitutive relationships

For the closure of the multiphase flow equations, a set of constitutive relationships is required in order to describe the secondary variables which are on dependent on the primary variables. We can distinguish between constitutive relations which describe the fluid properties, and those which quantify the interaction between the phases and the porous medium.

For the density, we can formulate the total differential as

$$\mathrm{d}\varrho = \varrho\beta_p \,\mathrm{d}p + \varrho\beta_T \,\mathrm{d}T \tag{3.17}$$

with the isothermal compressibility coefficient $\beta_p = (1/\varrho)\partial\varrho/\partial p$ and the isobaric volume expansion coefficient $\beta_T = (1/\varrho)\partial\varrho/\partial T$. Further, the water ($w$) phase is assumed to be incompressible, such that $\beta_{p_w} = 0$. For a gaseous phase (g) like air, we can calculate the density by assuming validity of the Ideal Gas law:

$$\varrho_g = \frac{p_g}{R_g T}, \tag{3.18}$$

where R_g is the individual gas constant obtained from

$$R_g = \frac{R_u}{M_g}, \tag{3.19}$$

with $R_u = 8.314$ J/(mole K) being the universal gas constant and the molecular weight M_g. For air, the gas constant is $R_{\text{air}} \approx 287$ J/(kg K).

The viscosity for all phases is mainly dependent on temperature. Thus, we use constant viscosities for the isothermal case. Several approaches can be found in the literature which consider temperature dependence. We use the relations given by [22].

For nonisothermal systems, we have to determine caloric state variables for the energy balance. The specific internal energy u_α represents the total energy of the molecules of phase α per unit mass. The specific enthalpy h_α is related with u_α by

$$h_\alpha = u_\alpha + \frac{p_\alpha}{\varrho_{\text{mass},\alpha}}. \tag{3.20}$$

For the water phase, the term $p_w/\varrho_{\text{mass},w}$ can be neglected compared to u_w and we approximate $u_w \approx h_w$. However, this term must be considered for the gas phase due its lower density. Values for the specific enthalpy and internal energy depend both on pressure and temperature and can be taken, for example, from the International Formulation Committee (1967) [22].

Up to now, we have discussed some properties of the fluid phases. Numerous values and functions describing them rather accurately can be found in the literature. The correct description of the interaction between fluid phases and the porous medium plays a key role in the description of the relationships for the capillary pressure and the relative permeabilities dependent on the phase saturations.

In recent years, a number of approaches has been developed for the description of the capillary pressure-saturation behavior of two fluid phases in a porous medium. Among the most well known approaches are those of Brooks and Corey (1964) [5] and of van Genuchten (1980) [41]. Both use parameterized functionals, which, however, differ characteristically if the wetting phase saturation approaches one ($S_w \to 1$). The Brooks–Corey (BC) approach is formulated as

$$p_c = p_d S_e^{-1/\lambda} \tag{3.21}$$

and the van Genuchten (VG) approach as

$$p_c = \frac{1}{\alpha}\left(S_e^{-1/m} - 1\right)^{1/n} \tag{3.22}$$

with

$$S_e = \frac{S_w - S_{w,r}}{1 - S_{w,r}} \tag{3.23}$$

and

$$m = 1 - \frac{1}{n}. \tag{3.24}$$

$S_{w,r}$ is the residual wetting phase saturation and S_e the effective saturation of the wetting phase. p_d, λ, α, and n are parameters, which can be determined by curve fitting to experimental data. Lenhard et al. (1989) [25] give a correlation between the BC (p_d, λ) and the VG (α, m, n) parameters.

There exist also numerous functions for the description of the relative permeability-saturation behavior. Again, among the most well-known are the Brooks–Corey and the van Genuchten approach, which can be derived from the corresponding capillary pressure functions by using pore network, respectively capillary tube, models according to Burdine (1953) [6] and Mualem (1976) [29]. The BC functions for the wetting and the non-wetting phases yield

$$k_{r,w} = S_e^{(2+3\lambda)/\lambda}, \tag{3.25}$$

$$k_{r,n} = (1 - S_e)^2\big(1 - S_e^{(2+\lambda)/\lambda}\big), \tag{3.26}$$

and the VG functions

$$k_{r,w} = \sqrt{S_e}\big[1 - \big(1 - S_e^{1/m}\big)^m\big]^2, \tag{3.27}$$

$$k_{r,n} = (1 - S_e)^{1/3}\big[1 - S_e^{1/m}\big]^{2m}. \tag{3.28}$$

4. Discretization

The forward problem is solved using the numerical simulator MUFTE-UG, where a vertex centered finite volume element method with fully implicit time discretization on unstructured meshes has been implemented [2,3,12]. In this method, the polyhedral domain Ω is divided into meshes $E_h = \{e_1, e_2, \ldots, e_k\}$ consisting of elements e_i with mesh width h. The set of vertices is denoted by $V = \{\nu_1, \nu_2, \ldots, \nu_n\}$, the location of vertex ν_i is $\mathbf{x}_i$ and the barycentre of element e_k is $\mathbf{x}^k$. Furthermore, $V(k)$ denotes the set of all indices i where ν_i is a corner of the element e_k and conversely $E(i)$ is the set of all indices k such that $i \in V(k)$. The secondary or dual mesh is constructed on the basis of E_h by connecting the element barycentres to the edge midpoints (figure 3). The

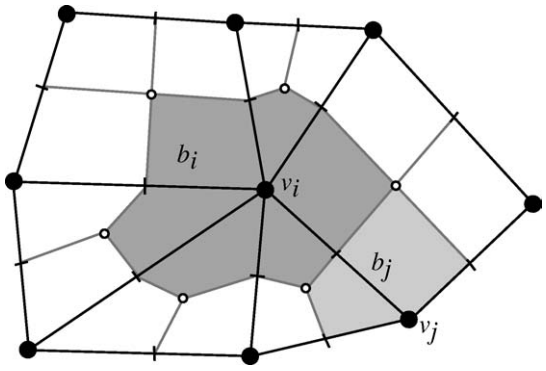

Figure 3. Control volume.

secondary mesh $B_h = \{b_1, b_2, \ldots, b_n\}$ consists of polyhedral regions b_i called *boxes* or *control volumes*. V_h is the space of lowest order conforming finite element functions or 'hat'-functions $\{\xi_i\}$ associated with E_h and W_h is the space of test functions which are the characteristic functions $\{\chi_i\}$ of the control volumes B_h. Thus for any $u_h \in V_h$ and $w_h \in W_h$ one has $u_h = \sum_{i\in E(i)} u_i \xi_i(\mathbf{x})$ and $w_h = \sum_{i\in E(i)} w_i \chi_i(\mathbf{x})$ with $u_i = u_h(\mathbf{x}_i)$ and $w_i = w_h(\mathbf{x}_i)$. Every finite element function $u_h \in V_h$ is identified with a vector $\mathbf{u} \in \mathbb{R}^N$ by a mapping $I_h : \mathbb{R}^N \to V_h$ in the usual way: $I_h(\mathbf{u}) = u_h$.

This semidiscrete formulation will lead to a system of ODEs. That is, for $0 < t < T^*$ one has to find the vectors $\mathbf{p}_g(t)$, $\mathbf{S}_w(t)$, $\mathbf{T}(t)$ such that for $\alpha = g, w, e$:

$$\frac{\mathrm{d}}{\mathrm{d}t}\mathbf{M}_\alpha(\mathbf{p}_g, \mathbf{S}_w, \mathbf{T}) + \mathbf{A}_\alpha(\mathbf{p}_g, \mathbf{S}_w, \mathbf{T}) + \mathbf{Q}_\alpha(t, \mathbf{p}_g, \mathbf{S}_w, \mathbf{T}) = 0. \tag{4.1}$$

The vector $\mathbf{M}_\alpha$ represents the accumulation term, $\mathbf{A}_\alpha$ the flux term and $\mathbf{Q}_\alpha$ the source/sink and boundary flux terms. This system can be formally rewritten as

$$\begin{pmatrix} M_{gg} & M_{gw} & M_{ge} \\ M_{wg} & M_{ww} & M_{we} \\ M_{eg} & M_{ew} & M_{ee} \end{pmatrix} \begin{pmatrix} \dfrac{\partial \mathbf{p}_g}{\partial t} \\ \dfrac{\partial \mathbf{S}_w}{\partial t} \\ \dfrac{\partial \mathbf{T}}{\partial t} \end{pmatrix} + \begin{pmatrix} \mathbf{A}_g(\mathbf{p}_g, \mathbf{S}_w, \mathbf{T}) + \mathbf{Q}_g(t, \mathbf{p}_g, \mathbf{S}_w, \mathbf{T}) \\ \mathbf{A}_w(\mathbf{p}_g, \mathbf{S}_w, \mathbf{T}) + \mathbf{Q}_w(t, \mathbf{p}_g, \mathbf{S}_w, \mathbf{T}) \\ \mathbf{A}_e(\mathbf{p}_g, \mathbf{S}_w, \mathbf{T}) + \mathbf{Q}_e(t, \mathbf{p}_g, \mathbf{S}_w, \mathbf{T}) \end{pmatrix} = 0, \tag{4.2}$$

with the (solution-dependent) submatrices given by

$$(M_{\alpha g})_{ij} = \frac{\partial \mathbf{M}_{\alpha g,i}}{\partial \mathbf{p}_{g,j}}, \qquad (M_{\alpha w})_{ij} = \frac{\partial \mathbf{M}_{\alpha w,i}}{\partial \mathbf{S}_{w,j}}, \qquad (M_{\alpha e})_{ij} = \frac{\partial \mathbf{M}_{\alpha e,i}}{\partial \mathbf{T}_j}.$$

In the case of isothermal two-phase flow, the variable T (temperature) will not appear and the submatrices will have dimension 2×2.

5. The parameter estimation problem

As we can see above, the governing partial differential equations or the constitutive relationships involve parameters representing the properties of fluids, the media or their interactions. In practical situations these parameters cannot be measured directly. Rather, they are to be determined from a set of observation data. Two types of methods have been reported, namely, direct and indirect methods (cf., e.g., [24]). In the direct methods, the parameters are determined by inverting the governing equations with simplified initial and boundary conditions using analytical or semi-analytical methods. This method has various limitations and cannot be applied to field-scale models. Indirect methods, on the other hand, are quite flexible and can be applied to practical problems. Our parameter identification technique is one of the indirect methods. In this technique, the direct problem is posed for prescribed but arbitrary initial and boundary conditions which can be solved by any appropriate analytical or numerical technique. The constitutive relationships intended to be applied are parametrized based on a-priori knowledge, and coefficients are determined by means of an optimization algorithm that extremizes

some objective function. The drawback of this method is that it cannot determine the specific form of the constitutive relationships and one has to presume some formulation of these relationships which holds to a sufficient degree of approximation. Many inverse problems are ill-posed which is characterized by non-uniqueness and instability [42], and this causes uncertainty of the determined parameters. This method also has the advantage that it is possible to obtain information concerning the parameter uncertainty from the estimation analysis.

The basic methodology explained here can be applied to a general parameter identification in nonstationary multiphase models. The current inverse modeling methodology is dominated by approaches which can be characterized by treating the multiphase simulation solver routine in the form of a black box, which just matches the unknown parameters (to be estimated) via a nonlinear process to an output least squares functional. This is the case, e.g., for ITOUGH/ITOUGH2 [15] and also in [8,23]. From the point of view of boundary value problems for nonstationary processes, this can be seen as a single shooting approach to the parameter identification problem, which, on the other hand, shares more properties with boundary value problems than pure initial value problems. As it is known that single shooting reveals instabilities for boundary value problems in ODE, a similar behavior has been observed with these black box approaches. Here, we use a multiple shooting approach similar to [36]. The multiple shooting by itself leads to a more robust solution behavior than a single shooting approach. The overall multiphase system solution technology is taken from the code MUFTE-UG (see above), which is enhanced by a multiple-shooting framework and computation of necessary derivatives.

5.1. Least-squares formulation

In order to perform a maximum likelihood estimation with respect to the output errors in measured data Z_{ij} of functions ϕ_{ij} of the variables S_w, p_g, and T, we formulate a pointwise weighted least squares function to be minimized,

$$\min \frac{1}{2} \sum_{i,j} \frac{(\phi_{ij}(p_g, S_w, T, \beta) - Z_{ij})^2}{\sigma_{ij}^2}. \tag{5.1}$$

Here, Z_{ij} are measurements of the saturation of water taken at the jth measurement time ($\hat{t}_j$) and the ith measurement position in space ($\hat{x}_i$). The measurement errors are assumed to be independently normally distributed with expectation 0 and standard deviation $\sigma_{i,j}$. This objective functional is subject to the conditions that the ODE (4.2) together with the suitable initial and boundary conditions are solved over the time horizon $[0, T^*] \ni \{\hat{t}_j\}_j$. The vector β collects the unknown parameters to be estimated.

5.2. The multiple shooting parameter estimation approach

We subdivide the time interval under consideration, $(0, T^*)$ into subintervals with the grid points $0 = \tau_0 < \tau_1 < \tau_2 < \cdots < \tau_m = T^*$, where in general the nodes $\{\tau_j\}$ are

independent from the measurement points in time. However, they typically include a subset of the measurement points and points with multipoint conditions $\{t_j\}$, if there exists any. For ease of presentation, however, we let the measurement time-grid coincide with the multiple shooting time-grid, since the necessary generalizations are obvious. At these nodes, the initial values of the state or differential variables S_j, p_j and T_j are introduced as unknowns in addition to the parameter vector β. In a standard multiple shooting formulation, these additional degrees of freedom are constrained by explicitly formulating continuity equations for the state variables. Thus, we arrive at the (time-) discretized least-squares problem

$$\min_{\{p_j,S_j,T_j\}_j,\beta} \frac{1}{2} \sum_{i,j} \frac{(\phi_{ij}(p_j, S_j, T_j, \beta) - Z_{ij})^2}{\sigma_{ij}^2} \tag{5.2}$$

subject to the continuity conditions

$$\begin{aligned} p_{j+1} - p_g(\tau_{j+1}; p_j, S_j, T_j, \beta) &= 0, \\ S_{j+1} - S_w(\tau_{j+1}; p_j, S_j, T_j, \beta) &= 0, \\ T_{j+1} - T(\tau_{j+1}; p_j, S_j, T_j, \beta) &= 0, \end{aligned} \tag{5.3}$$

for $j = 0, 1, \ldots, m-1$ and where $p_g(\tau_{j+1}; p_j, S_j, T_j, \beta)$, $S_w(\tau_{j+1}; p_j, S_j, T_j, \beta)$, $T(\tau_{j+1}; p_j, S_j, T_j, \beta)$ denote the solution at time τ_{j+1} of the multiphase ODE (4.2) with its initial and boundary conditions together with the additional initial conditions $S_w(\tau_j) = S_j$, $p_g(\tau_j) = p_j$ and $T(\tau_j) = T_j$.

In case of isothermal two phase flow, we only have the continuity condition for the variable saturation. The semidiscretization of equations (3.10) and (3.11) leads to a semi-explicit DAE where S_w is the differential variable and p_n is the algebraic variable. Otherwise the treatment remains the same.

5.3. A reduced generalized Gauss–Newton approach

An efficient numerical solution technique for the discretized parameter identification problem described in the previous section is the application of generalized Gauss–Newton methods as introduced in [4]. Increments to be added in each iteration are computed by solving the linearized constrained least squares problem

$$\min_{\{\Delta p_j,\Delta S_j,\Delta T_j\}_j,\Delta\beta} \frac{1}{2} \sum_{i=1}^{N} \sum_{j=0}^{m} \left\{ \phi_{ij}(p_j, S_j, T_j, \beta) - Z_{ij} + \left(\frac{\partial \phi_{ij}}{\partial p_j} \quad \frac{\partial \phi_{ij}}{\partial S_j} \quad \frac{\partial \phi_{ij}}{\partial T_j} \quad \frac{\partial \phi_{ij}}{\partial \beta} \right) \times \begin{pmatrix} \Delta p_j \\ \Delta S_j \\ \Delta T_j \\ \Delta \beta \end{pmatrix} \right\}^2 \Big/ \sigma_{ij}^2 \tag{5.4}$$

subject to

$$\begin{aligned} G_j^{pp}\Delta p_j + G_j^{ps}\Delta S_j + G_j^{pT}\Delta T_j - \Delta p_{j+1} + G_j^{p\beta}\Delta\beta = d_{j+1}^{p},\\ G_j^{sp}\Delta p_j + G_j^{ss}\Delta S_j + G_j^{sT}\Delta T_j - \Delta S_{j+1} + G_j^{s\beta}\Delta\beta = d_{j+1}^{s},\\ G_j^{Tp}\Delta p_j + G_j^{Ts}\Delta S_j + G_j^{TT}\Delta T_j - \Delta T_{j+1} + G_j^{T\beta}\Delta\beta = d_{j+1}^{T}, \end{aligned} \tag{5.5}$$

for $(j = 0, 1, 2, \ldots, m)$, where m is the number of shooting intervals, N is the number of measurements, G_j^{pp}, G_j^{ps}, etc. are the Wronskians which, for example, are given by

$$\begin{aligned} G_j^{sp} &= \frac{\partial S_w(\tau_{j+1};\, p_j, S_j, T_j, \beta)}{\partial p_j}, \qquad G_j^{ss} = \frac{\partial S_w(\tau_{j+1};\, p_j, S_j, T_j, \beta)}{\partial S_j},\\ G_j^{sT} &= \frac{\partial S_w(\tau_{j+1};\, p_j, S_j, T_j, \beta)}{\partial T_j}, \qquad G_j^{s\beta} = \frac{\partial S_w(\tau_{j+1};\, S_j, \beta)}{\partial \beta}, \quad \text{etc.} \end{aligned}$$

Equation (5.5) results from (5.3) due to the fact that the continuity conditions are not satisfied exactly at each of the shooting nodes during the iteration procedure. The Wronskians G_j^{kl} and $G_j^{k\beta}$ $(k, l \in \{s, p, T\})$ cannot be computed practically or even stored in the case of PDE. In order to avoid that, we apply a reduction technique, which has first been proposed in [31]. For the application to our case, we rewrite (5.5) as

$$\begin{pmatrix} G_j & G_j^{\beta} \end{pmatrix} \begin{pmatrix} \Delta_j \\ \Delta\beta \end{pmatrix} - \Delta_{j+1} = d_{j+1}, \tag{5.6}$$

where the block matrices and the vectors are given as

$$G_j = \begin{pmatrix} G_j^{pp} & G_j^{pT} & G_j^{pT} \\ G_j^{sp} & G_j^{ss} & G_j^{sT} \\ G_j^{Tp} & G_j^{Ts} & G_j^{TT} \end{pmatrix}, \quad G_j^{\beta} = \begin{pmatrix} G_j^{p\beta} \\ G_j^{s\beta} \\ G_j^{T\beta} \end{pmatrix}, \quad \Delta_j = \begin{pmatrix} \Delta p_j \\ \Delta S_j \\ \Delta T_j \end{pmatrix}, \quad d_j = \begin{pmatrix} d_j^{p} \\ d_j^{s} \\ d_j^{T} \end{pmatrix}.$$

Then we can solve (5.6) for Δ_{j+1} in recursion as

$$\Delta_{j+1} = -\sum_{l=1}^{j+1} \left(\prod_{i=l}^{j} G_i \right) d_l + \left\{ \sum_{l=1}^{j+1} \left(\prod_{i=l}^{j} G_i \right) G_{l-1}^{\beta} \right\} \Delta\beta + \prod_{i=0}^{j} G_i \Delta_0. \tag{5.7}$$

Since we assume to have full information on the initial data, we know $\Delta_0 = 0$, so that it can be neglected in the followng. Now the linear quadratic problem can be reformulated as an unconstrained quadratic problem,

$$\begin{aligned} \min_{\Delta\beta} \frac{1}{2} \Bigg[\sum_{i=1}^{N} \sum_{j=0}^{m} \Bigg\{ \phi_{ij}(p_j, S_j, T_j, \beta) - Z_{ij} - \begin{pmatrix} \frac{\partial \phi_{ij}}{\partial p_j} & \frac{\partial \phi_{ij}}{\partial S_j} & \frac{\partial \phi_{ij}}{\partial T_j} \end{pmatrix} g_j^{s} \\ + \left(\begin{pmatrix} \frac{\partial \phi_{ij}}{\partial p_j} & \frac{\partial \phi_{ij}}{\partial S_j} & \frac{\partial \phi_{ij}}{\partial T_j} \end{pmatrix} g_j^{\beta} + \frac{\partial \phi_{ij}}{\partial \beta} \right) \Delta\beta \Bigg\}^2 \Bigg], \end{aligned} \tag{5.8}$$

where

$$g_j^s = \sum_{l=1}^{j} \left(\prod_{k=l}^{j} G_k \right) d_l, \tag{5.9}$$

$$g_j^\beta = \sum_{l=1}^{j} \left(\prod_{k=l}^{j} G_k \right) G_{l-1}^\beta. \tag{5.10}$$

The vector g_j^s and the matrix g_j^β can be computed simultaneously to the solution of the forward multiple shooting sweep in each nonlinear iteration. This QP is solved for the parameter vector increment $\Delta\beta$. The Levenberg–Marquardt technique [26,28] has been used for the solution of the QP. Afterwards, the increments can be obtained from the recursion

$$\Delta_{j+1} = G_j \Delta_j + G_j^\beta \Delta\beta - d_{j+1}.$$

These increments are then scaled by a line-search parameter and added to the current iterate.

5.4. Computation of derivatives

For the solution of the linear quadratic subproblems of the previous section, we need the matrix–vector products with the Wronskians G_j, G_j^β. These can be carried out "on the fly" (*internal numerical differentiation* [4,36]) by solving linear systems of equations with the same linear solver which is used for the integration of the ODE. The differentiation of the ODE (4.2) with respect to p_g, S_w, and T leads to the same matrix which is used in the formulation of linear systems resulting from the application of a Newton method to the implicit equation defined by, e.g., an implicit Euler method. Therefore, the necessary computations to be carried out in each integration step for the computation of G_j, G_j^β are $\dim(\beta)$ additional solutions of linear systems after each completed nonlinear Newton step, with the same matrix as has been used in the last Newton step, and with the same linear solver (here a multigrid solver), for details see [17,18].

6. Numerical results and discussion

6.1. Two-phase flow (isothermal case)

We consider the *McWhorter problem* (cf. [19, p. 258]) in the domain $\Omega = [0, 2.6] \times [0, 1.0]$ and the time interval $(0, 1000$ [s]) as a test case for the verification of our algorithm. This problem deals with the computation of the instationary displacement process of oil by water, taking into account the capillary effects in a one-dimensional horizontal system (figure 4). The fluid and solid matrix properties, constitutive relationships and simulation parameters are given as follows.

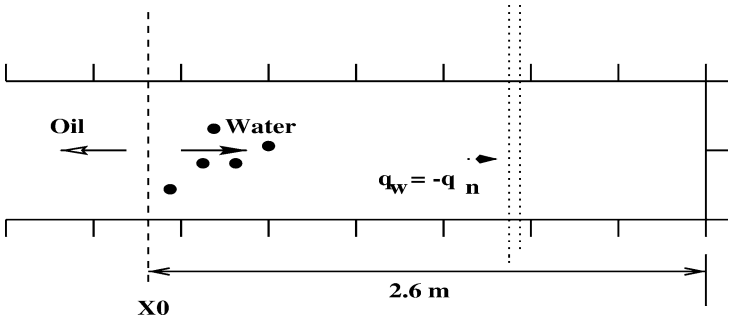

Figure 4. McWhorter problem (cf. [19]).

Table 2
Fluid and solid matrix properties and constitutive relationships.

		Water	Oil
(1)	fluid properties		
	density	1000 [kg/m^3]	1000 [kg/m^3]
	dyn. viscosity	0.001 [kg/(ms)]	0.001 [kg/(ms)]
(2)	solid matrix properties and constitutive relationships		
	abs. permeability k	[m^2]	$a \cdot 10^{-10}$ a: to be estimated
	porosity ϕ	[–]	0.30
	pore size distr. index λ	[–]	to be estimated
	entry pressure p_d	[Pa]	5000
	residual saturation $s_{\alpha r}$	0.00	0.00
	rel. permeability $k_r(S_w)$	[–]	Brooks–Corey model
	capillary pressure $pc(S_w)$	[Pa]	Brooks–Corey model

- Boundary conditions: water saturation $S_w = 1.0$ [–], oil pressure $p_n = 2 \cdot 10^5$ [Pa] at $x = 0$,

$$\rho_\alpha \mathbf{v}_\alpha \cdot \eta = 0 \quad \text{at } y = 0\,[\text{m}],\ y = 1.0\,[\text{m}] \text{ and } x = 2.6\,[\text{m}].$$

- Initial condition: water saturation $S_w(x, 0) = 0.01$ [–] for $x \in \Omega$.

We identify the parameter λ, in the Brooks–Corey relationship for capillary pressure and relative permeabilities, as discussed in section 3.2, and a, the scaling factor in the absolute permeability. Since we do not have actual experimental or measurement data for this type of problem, we have used the "artificial" data. That is, the capillary pressure values obtained by the numerical computation using $\lambda = 2$ and $a = 1$ have been used as measurement values for this case. These values of parameters were used in the numerical computations in [19] for a comparison with quasi-analytic solutions. Five such measurement points (marked in black in figure 4) and three shooting intervals are used for the computation at times 3.75 [s] and 31.15 [s]. All the measurement points are taken within the region between the boundary at $x = 0$ and the "free boundary"

Table 3
Stability of solution for the estimation of λ and a.

Data set	# iter.	Value of λ	Value of a
actual data	7	2.000 ± 0	0.999 ± 0
data with 5% error	7	1.987 ± 0.014	0.973 ± 0.030
data with 10% error	7	1.979 ± 0.027	0.979 ± 0.055

(which moves with time) at time 31.15 [s]. We use the MUFTE-UG [20] software tool for solving the above mentioned set of partial differential equations on a grid with 1305 grid points. The least-squares problem is solved using reduced Gauss–Newton technique, which is incorporated in MUFTE-UG. Each iteration of the multiple-shooting takes about 2 seconds of CPU time for the above grid size on an SGI machine. The iterations are stopped when $\|(\Delta\lambda, \Delta a)\|_2 < 10^{-3}$.

The solution is independent of the initial guess of the saturation. Table 3 presents the results of the computation by using the actual measurements and measurements with a random error of 5 and 10% with starting values of $\lambda = 1.6$ and $a = 0.5$. As we can see, the change in the final value of the parameters (λ, a) is approximately $(0.7\%, 2.7\%)$ and $(1.05\%, 2.1\%)$, respectively. Figure 5 presents the results of the saturations of two shooting intervals in different iterations. The defects in the computations are initially large and are reduced in the subsequent iterations, as expected. As we have already mentioned, it is possible to determine the "measure of goodness" of the parameters or the parameter uncertainty by this method. Since the term

$$\left(\frac{\partial \phi_{ij}}{\partial S_j} g_j^{\beta} + \frac{\partial \phi_{ij}}{\partial \beta}\right)$$

in (5.8) is computed in each iteration, all information necessary for the computation of linearized variances and covariances for the parameters are available if the parameter identification algorithm is converged (and therefore $d_j = 0,\ \forall j$). If a parameter P_i lies in the interval $P_i \in (\widehat{P}_i - \delta_i, \widehat{P}_i + \delta_i)$, then δ_i is determined by using the formula (for details, see [4])

$$\delta_i = \|F_1\|_2 \left(\sigma_{ii} \frac{l_1}{l_2} F_{1-\alpha}(l_1, l_2)\right)^{1/2}, \tag{6.1}$$

where $\|F_1\|_2$ is the 2-norm of the linearized objective function, l_1 is the number of parameters, $l_2 = \dim F_1 - l_1$, σ_{ii} is the variance of the parameter P_i, and $F_{1-\alpha}$ is the $(1-\alpha)$-quantile of the F-distribution. Based on this, we compute 95% confidence intervals and display them in table 3, as well.

6.2. Non-isothermal case

6.2.1. Experimental setup

For the parameter identification in highly coupled flow and transport processes linked with heat and mass transfer between the phases, the one-dimensional experiments

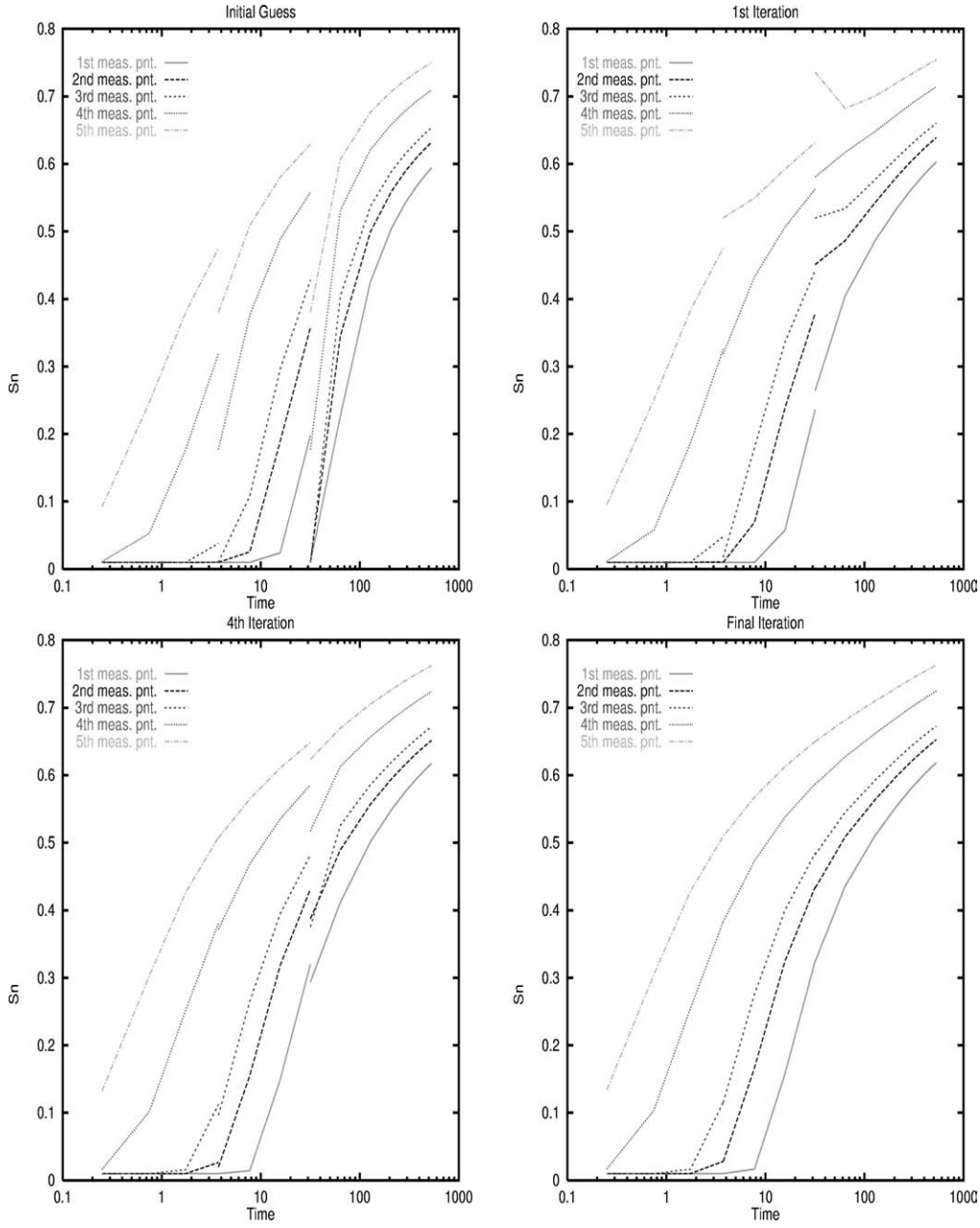

Figure 5. Saturation of non-wetting phase at different iterations.

are most practical. We have applied our method to one of these experiments for the simulation and identification. The experiment was carried out in a vertically positioned, sand filled column in the VEGAS research facility at the University of Stuttgart, Ger-

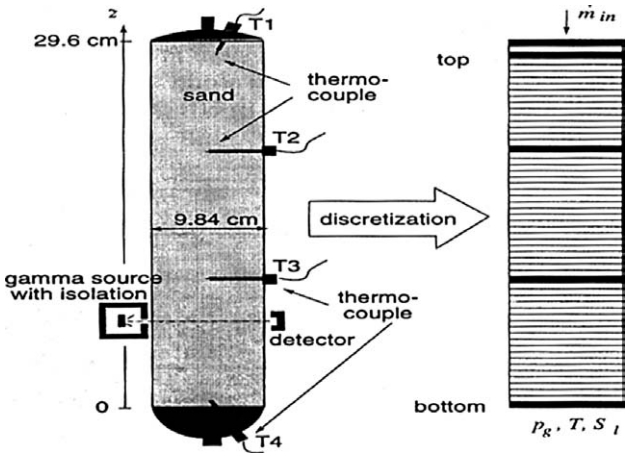

Figure 6. Experimental setup (according to [9]).

many. The motivation for this experiment was to carry out an experimental program in order to find criteria for the optimization of thermally enhanced soil vapor extraction as an efficient technology for the remediation of NAPL-contaminated unsaturated soils. Small-scale laboratory experiments represent an important part of the experimental program for the investigation of the thermodynamical and hydraulic processes and for the quantification and identification of the dominating processes. The one-dimensional setup of the column experiment facilitates the understanding of the complex coupled processes. In the one-dimensional case, the heat flow is less sensitive to heterogeneities on the microscale, while relative permeability and capillary pressure have a stronger influence on the overall flow. The phase saturation of the water phase was measured by the principle of gamma absorption. The detailed description of the experiments (shown in figure 6) are given in [13].

6.2.2. Constitutive relationships and initial/boundary conditions

The mathematical relationship between capillary pressure and saturation in the sand is used which is according to *Van Genuchten* [41], as discussed in section 3.2, since this produces a good fit to the capillary pressure-saturation measurement data for the coarse sand (cf. [21]). The fluid and solid matrix properties are used as given in table 4. The initial temperature for the experiment was 20°C. The steam flow was injected at $z = 296$ mm with a *Neumann*-boundary condition. Temperature, pressure, and saturation of the gas phase were fixed to a constant value (*Dirichlet*-boundary condition).

We have identified the parameter n in the *van Genuchten* relationship for capillary pressure and relative permeabilities, and a, the *scaling factor* in the absolute permeability. We have used the MUFTE_UG [20] software tool for solving the above mentioned set of partial differential equations. The least-squares problem is solved by the reduced Gauss–Newton technique, which is incorporated in MUFTE-UG. The iterations are stopped when $\|\text{gradient}\|_2 < 10^{-4}$.

Table 4
Fluid and solid matrix properties and constitutive relationships.

(1)	fluid properties (water)	
	density	1000 [kg/m^3]
	dyn. viscosity	0.001 [kg/(ms)]
(2)	solid matrix properties (sand)	
	density ρ_s	2650 [kg/m^3]
	abs. permeability k	$a \cdot 10^{-10}$ m^2
		a: to be estimated
	porosity ϕ	0.3678
	residual saturation water S_{wr}	0.1
	residual saturation air S_{gr}	0.05
	heat capacity C_s	840 [J/(kg K)]
	heat conductivity $\lambda_{pm}^{S_w=0}$	0.35 [J/(s m K)]
	heat conductivity $\lambda_{pm}^{S_w=1}$	1.8 [J/(s m K)]
	van Genuchten parameter $1/\alpha$	663.13 [/Pa]
	van Genuchten parameter n	to be estimated

Table 5
Stability of the solution for the estimation of n and a.

Data set	# iter.	Value of n	Value of a
actual data	17	4.000 ± 0	1.000 ± 0
data with 5% error	17	3.9747 ± 0.0007	1.0293 ± 0.0008
data with 10% error	17	3.9648 ± 0.0014	1.0414 ± 0.0016

6.2.3. Use of synthetic data

In order to avoid the ambiguity due to uncertainty in the experimental data that might affect the numerical model, we use synthetic data generated by using fixed values of the parameters $n = 4.0$ and $a = 1.0$ for the verification of the model. 54 of such data from four shooting intervals at times $\tau = \{766, 1534, 2238\}$ are used. Afterwards, a random error of 5 and 10% is added to these data and used in the subsequent runs. The results for the initial guess of the parameters ($n = 3.75, a = 0.75$) are displayed in table 5. The change in the final parameter (n, a) values is (0.63%, 2.93%) and (0.88%, 4.14%), respectively.

6.2.4. Use of experiment: steam injection into wet coarse sand from the top

This experiment has a constant mass flow injection of 0.18 kg/h steam with a quality of ≈90%. 43 measurements of water saturation from four positions in space, e.g., $z = \{200, 180, 150, 130\}$ mm and at different times $t \in [830, 1600]$ seconds have been used in the four shooting intervals at times $\tau = \{1023, 1231, 1599\}$ seconds. The initial distribution of saturation used in the experiment and in the numerical computation is shown in figure 7. The saturation at the upper part of the column indicates a nearly residual saturation, while there is still a storage capacity of approximately 40% to 70% in the bottom region ($z = 30$ mm).

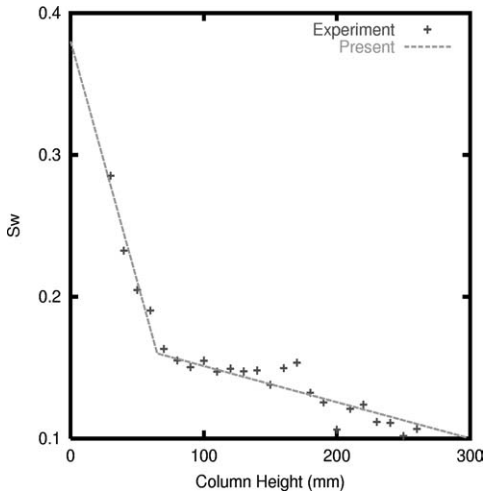

Figure 7. Initial saturation of water.

Table 6
Stability of solution for the estimation of n and a.

No. of exp.	Parameter	Initial guess	Estimated value
1	n	4.0	3.264817 ± 0.005329
	a	0.5	0.544405 ± 0.005059
2	n	3.5	3.264943 ± 0.005329
	a	0.75	0.544321 ± 0.005060
3	n	3.0	3.263355 ± 0.005336
	a	1.0	0.545413 ± 0.005044
4	n	2.5	3.263370 ± 0.005336
	a	0.65	0.545404 ± 0.005044
5	n	3.0	3.262310 ± 0.005341
	a	0.25	0.546120 ± 0.005034

We have computed the solutions for five different sets of the initial guesses, in order to show for the parameters that the converged solution does not depend on the initial guess (some kind of stability of the solution, as the theoretical analysis for this nonlinear case is beyond consideration). The 95% confidence interval of the estimated parameters is also computed by using (6.1) based upon the linearized variance and covariance matrix. In all the five cases this is less than (± 0.0054) for the parameter n and (± 0.0051) for the parameter a. From the results of the computations displayed in table 6 we can say that we have achieved relatively stable estimates of the parameters. The cost of computations is between 30 to 60 direct runs in all the five cases where each direct run requires about 45 seconds of CPU time on an Intel(R) Xeon(TM) 1700 MHz machine. Figure 8 presents the results of different iterations (for $n = 2.5$ and $a = 0.65$) where the water saturations have been computed at different times. The discontinuities of the solutions

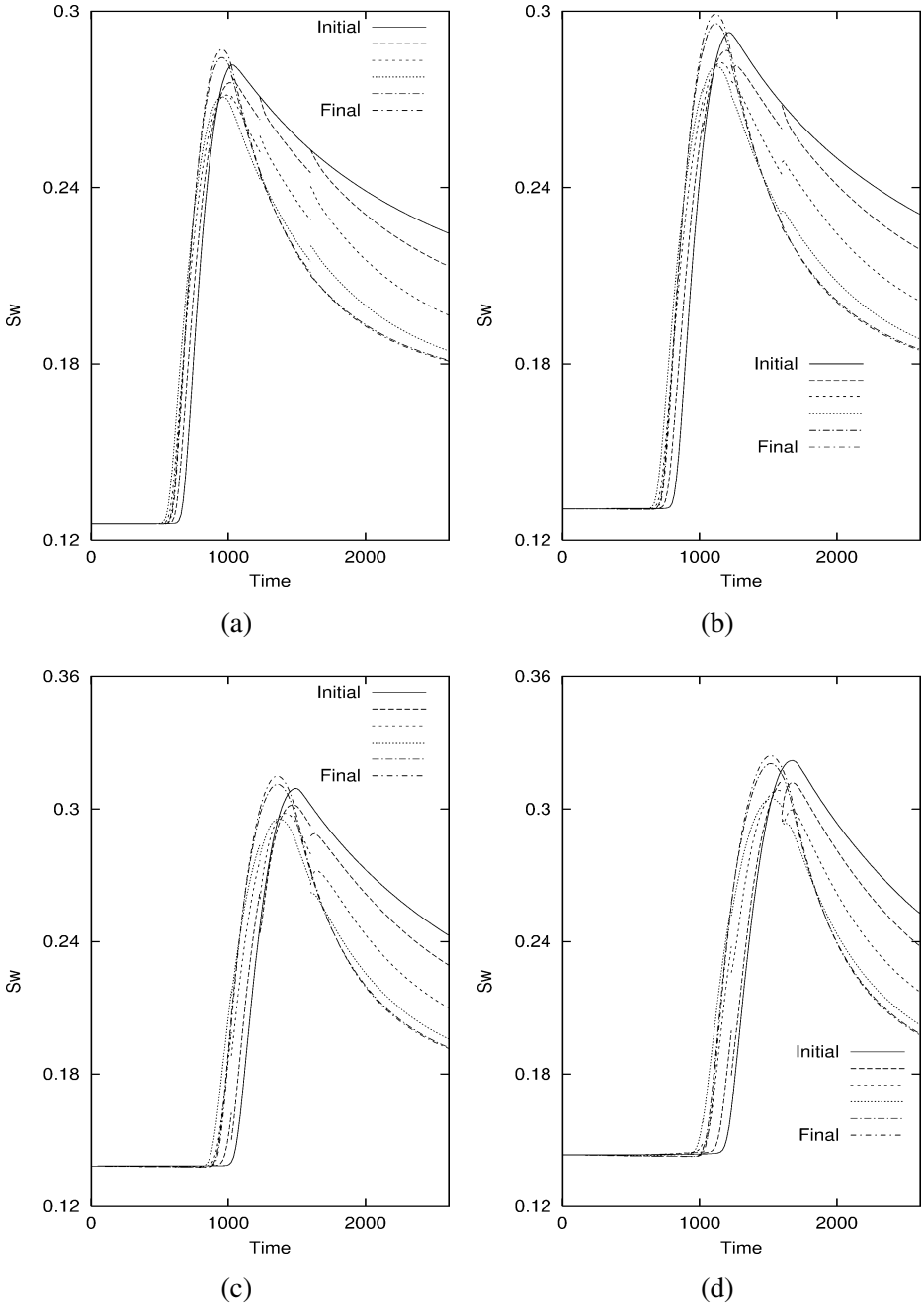

Figure 8. Convergence history at the points $Z = 200$ mm (a), 180 mm (b), 150 mm (c) and 130 mm (d).

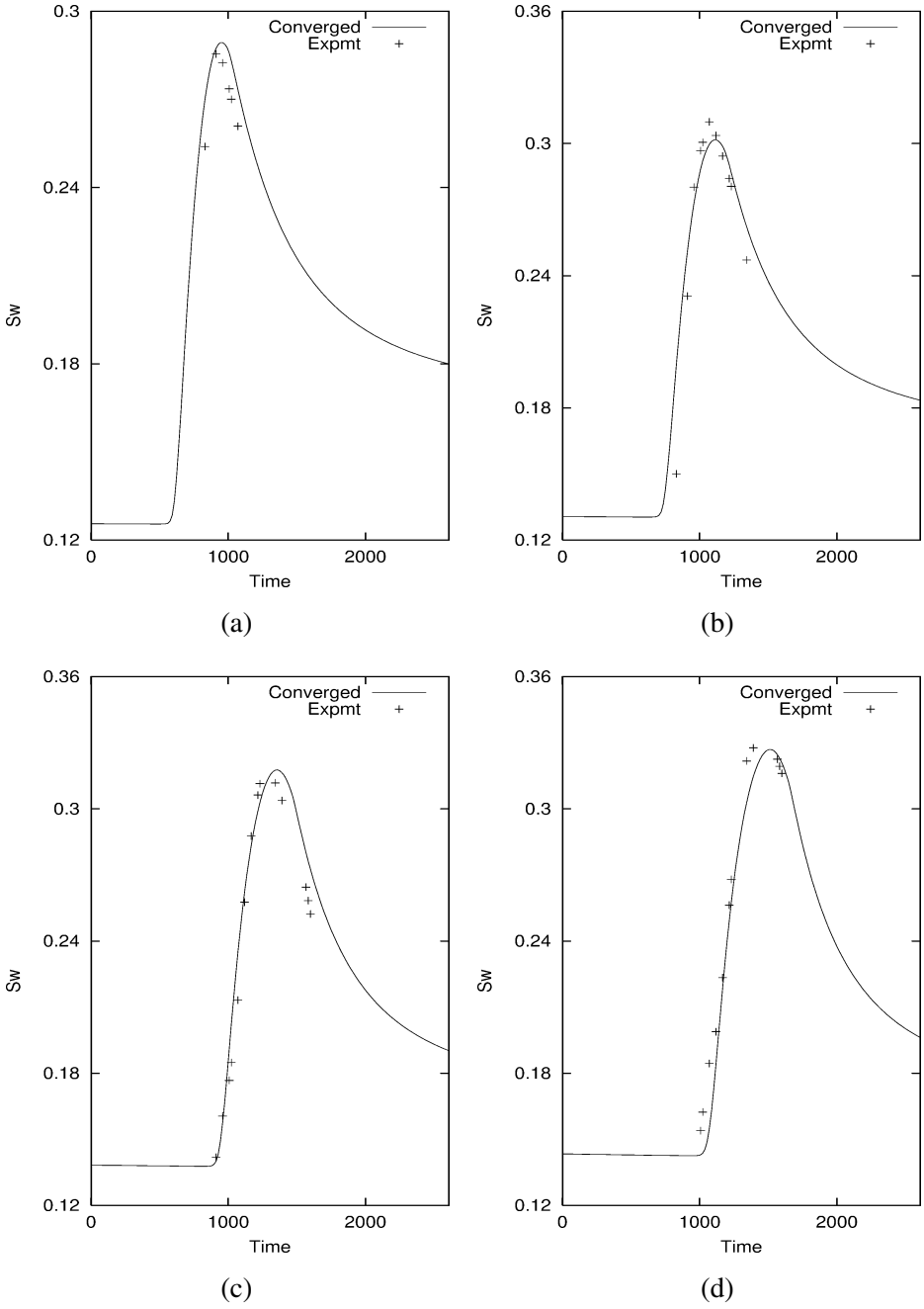

Figure 9. Comparison of computed and used experimental water saturation in the column at $Z =$ 200 mm (a), 180 mm (b), 150 mm (c) and 130 mm (d).

at the shooting interval represent the values of the defects (d_i), which are larger during the beginning of the iterations and become zero when we get to the converged solutions of the parameter.

Figure 9 presents the comparison of the converged numerical solution with the *used* experimental data. As we can see, there is excellent agreement of the solution.

Figure 10 presents the comparison of the converged solution with the additional experimental data in the downstream (*) at the column height $z = 130$ mm. As we can see here, the numerical solution does not match very well towards the downstream (approximately, after a time of 2000 seconds). This means that the gravity driven drainage process in the experiment does not match with that of the numerical computation. Several reasons are possible for this mismatch. First, we should keep in mind that the mathematical model uses the same capillary pressure–saturation relationship for both imbibition and drainage, which is not the case in reality, an effect that is called hysteresis. This hypothesis is also offered by similar experiments and inverse computations described in [9]. Another reason can be that the injection rate is not included in the set of estimated parameters here. As shown in [9], the rate of mass flow injected into the sand strongly affects the propagation of the steam/condensation front since it is directly correlated with the amount of thermal energy required for the heating of the sand. [21] describe the numerical simulation of the same experiment with a different set of data without using inverse modeling, but applying a trial-and-error method instead in order to obtain the best fit between measurements and simulated data. When using an inverse model with an automatic minimization of the objective function, one must be aware

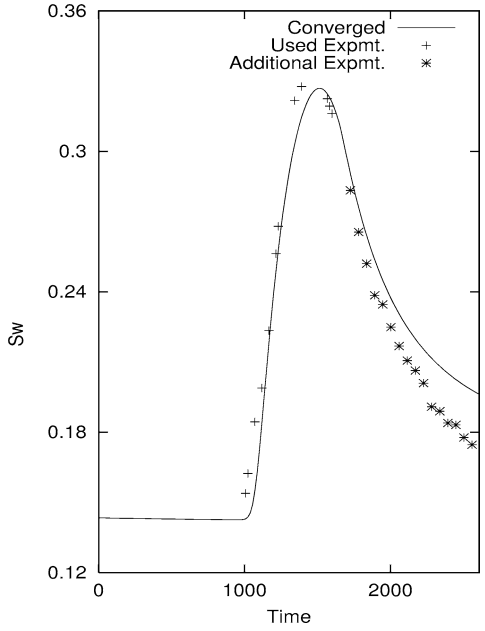

Figure 10. Comparison of computed and experimental water saturation in the column at $Z = 130$ mm.

that the minimization algorithm always focuses on regions with steep fronts (peaks), because already small deviations between measurements and simulated data will cause large residuals. This is the reason why the results obtained in this paper are difficult to compare with those in [21]. Nevertheless, we strongly recommend to include hysteresis effects into the forward model. Following the arguments given above and considering that the results of [9] indicate effects of hysteresis although including the injection rate into the set of estimated parameters, it is likely that the results improve if hysteresis effects are incorporated in the model.

7. Conclusions

An algorithm has been developed for parameter identification in multiphase flow through porous media. It employs the reduced Gauss–Newton method to an output least squares minimization problem in an efficient implementation. Special care has been taken concerning the proper formulation of continuity conditions and the computation of derivatives. The numerical studies show that the method is comparatively stable (small changes in experimental data result in similar changes in the solution).

The numerical results indicate that the modeling concept applied within this work lacks certain effects which are due to hysteresis. The methodology built up so far gives reasonable results. It, however, can be improved by incorporating this additional effect, which has not been part of the program of this work. Here, we would like to add some comments on hysteresis.

In multiphase systems one can distinguish between two kinds of displacement processes. A drainage process is given when a non-wetting fluid displaces a wetting fluid. In the case of imbibition, the wetting fluid displaces the non-wetting fluid. The curves of the capillary pressure–saturation and relative permeability–saturation relationships differ between a drainage and an imbibition. This phenomenon is called hysteresis.

Different effects on the microscale are responsible for the hysteretic behavior in porous media multiphase flow, e.g., contact angle, pore geometry (ink-bottle effect), fluid entrapment, see [38]. In order to consider hysteresis effects on the macroscale, it is necessary to define the curves shown in figure 11. E.g., the main drainage curve (MDC) is valid if the porous medium is initially filled with the wetting phase; thus, the capillary pressure is $p_c = 0$. The non-wetting phase displaces the wetting phase and the capillary pressure increases with a decreasing wetting-phase saturation along the MDC. Accordingly, the other curves must be defined and the history of the drainage/imbibition processes must be monitored. Approaches like that of Parker and Lenhard (1987) [30] often use a semi-empirical scaling of the capillary pressure curves. They introduce additional parameters which must be determined a priori or may be determined by inverse modeling. For future, we plan to investigate if inverse modeling can be used in order to determine such effects quantitatively.

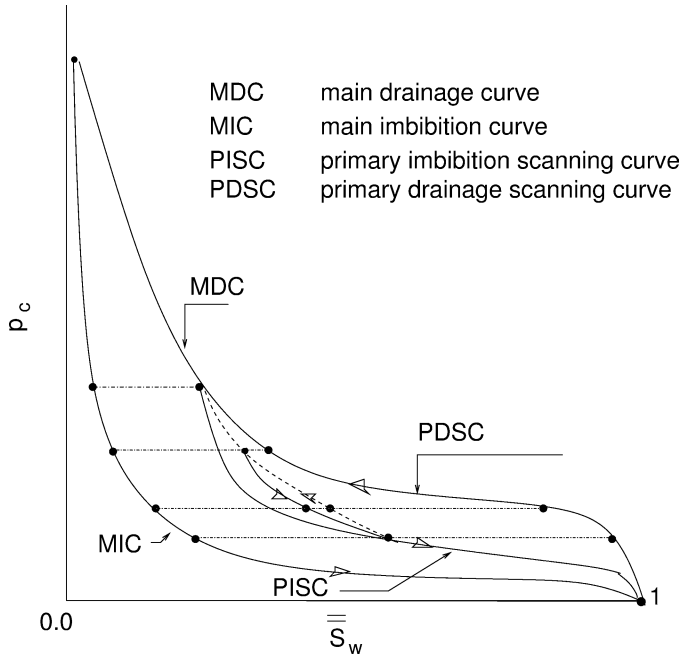

Figure 11. Hysteresis of the capillary pressure–saturation relationship according to [38].

Acknowledgements

This research was partly supported by the German National Science Foundation (DFG). The authors are indebted to G. Wittum for invaluable discussions, to P. Bastian for co-operations on UG, and to A. Faerber for the experimental data. We would also like to thank anonymous referees for their comments and suggestions which have improved the exposition substantially.

References

[1] Y. Bard, *Nonlinear Parameter Estimation* (Academic Press, New York, 1974).
[2] P. Bastian, Numerical computation of multiphase flows in porous media, Habilitationsschrift, Technische Fakultät der Christian-Albrechts-Universität Kiel, Kiel (1999).
[3] P. Bastian and R. Helmig, Efficient fully-coupled solution techniques for two-phase flow in porous media: Parallel multigrid solution and large scale computations, Adv. in Water Resour. 23 (1999) 199–216.
[4] H.G. Bock, Randwertproblemmethoden zur Parameteridentifizierung in Systemen nichtlinearer Differentialgleichungen, Bonner Mathematische Schriften 183 (1987).
[5] A. Brooks and A. Corey, Hydraulic properties of porous media, in: *Hydrol. Pap.*, Colorado State University, Fort Collins, 1964.
[6] N. Burdine, Relative permeability calculations from pore–size distribution data, Technical Report, Petroleum Transactions, AIME (1953).

[7] J. Carrera and S.P. Neuman, Estimation of aquifer parameters uder transient and steady state conditions, 1. Maximum likelihood method incorporating prior information, Water Resour. Res. 22(2) (1986) 199–210.
[8] G. Chavent, J. Jaffré, S. Jegou and J. Liu, A symbolic code generator for parameter estimation, in: *Proc. of the SIAM Workshop on Computational Differentiation*, SIAM, 1996, pp. 129–136.
[9] H. Class, Theorie und numerische Modellierung nichtisothermer Mehrphasenprozesse in NAPL-kontaminierten porösen Medien, Ph.D. thesis, Mitteilungsheft 105, Institut für Wasserbau, Universität Stuttgart (2001).
[10] H. Class, R. Helmig and P. Bastian, Numerical simulation of nonisothermal multiphase multicomponent processes in porous media, 1. An efficient solution technique, Adv. in Water Resour. 25 (2002) 533–550.
[11] Th. Dreyer, B. Maar and V. Schulz, Multigrid optimization in applications, J. Comput. Appl. Math. 120(1/2) (2000) 67–84.
[12] R.E. Ewing, R.D. Lazarov and Y. Lin, Finite volume element approximations of nonlocal in time one-dimensional flows in porous media, Computing 64 (2000) 157–183.
[13] A. Faerber, Wärmetransport in der ungesättigten Bodenzone: Entwicklung einer thermischen in-situ Sanierungstechnologie, Dissertation, Institut für Wasserbau, Universität Stuttgart (1997).
[14] I. Fatt and W.A. Klikoff, Effect of fractional wettability on multiphase flow through porous media, AMIE Transactions 216 (1959) 246.
[15] S. Finsterle, Multiphase inverse modeling: An overview, in: *Proceedings, DOE Geothermal Program Review XVI*, Berkeley, CA, 1–2 April 1998, pp. 3-3–3-9.
[16] S. Finsterle and K. Pruess, Solving the estimation-identification problem in two-phase flow modeling, Water Resour. Res. 31(4) (1995) 913–924.
[17] S.B. Hazra and V. Schulz, Numerical parameter identification in multiphase flow through porous media, J. Comput. Visual. Sci. 5 (2002) 107–113.
[18] S.B. Hazra and V. Schulz, On efficient computation of the optimization problem arising in the inverse modeling of nonstationary multiphase multicomponent flow through porous media, Comput. Opt. Appl. (2004) to appear.
[19] R. Helmig, *Multiphase Flow and Transport Processes in the Subsurface – a Contribution to the Modeling of Hydrosystems* (Springer, Berlin, 1997).
[20] R. Helmig, H. Class, R. Huber, H. Sheta, J. Ewing, R. Hinkelmann, H. Jakobs and P. Bastian, Architecture of the modular program system MUFTE_UG for simulating multiphase flow and transport processes in heterogeneous porous media, Math. Geologie 2 (1998).
[21] R. Helmig, H. Class, A. Faerber and M. Emmert, Heat transport in the unsaturated zone – comparison of experimental results and numerical simulations, J. Hydr. Reas. 36(6) (1998).
[22] International Formulation Committee, A formulation of the thermodynamic properties of ordinary water substance, Technical Report, IFC Sekretariat, Düsseldorf, Germany (1967).
[23] P. Knabner and B. Igler, Structural identification of nonlinear coefficient functions in transport processes through porous media, in: *Lectures on Applied Mathematics*, eds. Bungartz, Hans-Joachim et al. (Springer, Berlin, 1999) pp. 157–175.
[24] J.B. Kool, J.C. Parker and M.Th. Van Genuchten, Parameter estimation for unsaturated flow and transport models – A review, J. Hydrology 91 (1987) 255–293.
[25] R. Lenhard, J. Parker and S. Mishra, On the correspondence between Brooks–Corey and Van Genuchten models, J. Irrigation Drainage Engrg. 115(4) (1989) 744–751.
[26] K. Levenberg, A method for the solution of certain nonlinear problems in least squares, Quart. Appl. Math. 2 (1944) 164–168.
[27] M.C. Leverett, Capillary behaviour in porous solid, AMIE Transactions 142 (1941) 152.
[28] D.W. Marquardt, An algorithm for least squares estimation of nonlinear parameters, J. Soc. Ind. Appl. Math. 11(2) (1963) 431–441.

[29] Y. Mualem, A new model for predicting the hydraulic conductivity of unsaturated porous media, Water Resour. Res. 12 (1976) 513–522.
[30] J. Parker and R. Lenhard, A model for hysteretic constitutive relations governing multiphase flow, 1. Saturation–pressure relations, Water Resour. Res. 23(12) (1987) 2187–2196.
[31] J. Schlöder, Numerische Methoden zur Behandlung hochdimensionaler Aufgaben der Parameteridentifizierung, Bonner Mathematische Schriften 187 (1988).
[32] V. Schulz, Solving discretized optimization problems by partially reduced SQP methods, Comput. Visul. Sci. 1 (1998) 83–96.
[33] V. Schulz, Constrained programming for optimization problems in PDE, in: *ENUMATH 97, Proc. of the 2nd European Conf. on Numerical Mathematics and Advanced Applications*, eds. H.G. Bock, G. Kanschat, R. Rannacher, F. Brezzi, R. Glowinski, Y.A. Kuznetsov and J. Periaux (World Scientific, Singapore, 1998) pp. 580–587.
[34] V. Schulz, Mehrgittermethoden für Optimierungsprobleme bei partiellen Differentialgleichungen, Habilitationsschrift, Universität Heidelberg (2000).
[35] V. Schulz, A. Bardossy and R. Helmig, Conditional statistical inverse modeling in groundwater flow by multigrid methods, Comput. Geosci. 3 (1999) 49–68.
[36] V. Schulz, H.G. Bock and M. Steinbach, Exploiting invariants in the numerical solution of multipoint boundary value problems for DAEs, SIAM J. Sci. Comput. 19(2) (1998) 440–467.
[37] V.H. Schulz and G. Wittum, Multigrid optimization methods for stationary parameter identification problems in groundwater flow, in: *Multigrid Methods V*, eds. W. Hackbusch and G. Wittum, Lecture Notes in Computational Science and Engineering, Vol. 3 (Springer, New York, 1998) pp. 276–288.
[38] H. Sheta, Einfluss der Hysterese bei Infiltrations- und Ausbreitungsvorgängen in der gesättigten und ungesättigten Bodenzone, Ph.D. thesis, Universität Stuttgart, Institut für Wasserbau (1999).
[39] F. Stauffer, W. Kinzelbach, K. Kovar and E. Hoehn, eds., *ModelCARE'99, Internat. Conf. on Calibration and Reliability in Groundwater Modelling*, Vol. 265 (IAHS Publication, 2000).
[40] K.S. Udell and J.S. Fitch, Heat and mass transfer in capillary porous media considering evaporation, condensation and non-condensible gas effects, presented at: *23rd ASME/AIChE National Heat Transfer Conference*, Denver, CO, August 1985.
[41] M.T. van Genuchten, A closed form equation for predicting the hydraulic conductivity of unsaturated soils, Soil Sci. Soc. Amer. J. 44(5) (1980) 892–898.
[42] W.G. Yeh, Review of parameter estimation procedures in groundwater hydrology: The inverse problem, Water Resour. Res. 22 (1986) 95–108.